Measurements and simulations of microscopic damage to DNA in water by 30 keV electrons: A general approach applicable to other radiation sources and biological targets

Marc Benjamin Hahn*
Institut für Experimentalphysik, Freie Universität Berlin, D-14195 Berlin, Germany
and Bundesanstalt für Materialforschung und Prüfung, D-12205 Berlin, Germany

Susann Meyer
Institute of Biochemistry and Biology, University of Potsdam, D-14476 Potsdam, Germany
and Bundesanstalt für Materialforschung und Prüfung, D-12205 Berlin, Germany

Hans-Jörg Kunte and Tihomir Solomun†
Bundesanstalt für Materialforschung und Prüfung, D-12205 Berlin, Germany

Heinz Sturm
Bundesanstalt für Materialforschung und Prüfung, D-12205 Berlin, Germany
and Technical University Berlin, D-10587 Berlin, Germany
(Received 9 February 2017; published 30 May 2017)

The determination of the microscopic dose-damage relationship for DNA in an aqueous environment is of a fundamental interest for dosimetry and applications in radiation therapy and protection. We combine GEANT4 particle-scattering simulations in water with calculations concerning the movement of biomolecules to obtain the energy deposit in the biologically relevant nanoscopic volume. We juxtaposition these results to the experimentally determined damage to obtain the dose-damage relationship at a molecular level. This approach is tested for an experimentally challenging system concerning the direct irradiation of plasmid DNA (pUC19) in water with electrons as primary particles. Here a microscopic target model for the plasmid DNA based on the relation of lineal energy and radiation quality is used to calculate the effective target volume. It was found that on average fewer than two ionizations within a 7.5-nm radius around the sugar-phosphate backbone are sufficient to cause a single strand break, with a corresponding median lethal energy deposit being $E_{1/2} = 6 \pm 4$ eV. The presented method is applicable for ionizing radiation (e.g., γ rays, x rays, and electrons) and a variety of targets, such as DNA, proteins, or cells.

DOI: 10.1103/PhysRevE.95.052419

I. INTRODUCTION

The investigation of radiation induced damage is performed for a wide range of radiation sources and different experimental geometries. Thereby, continuous x rays [1], laser pulses [2,3], or electrons [4–8] are used to irradiate biomolecules. The irradiations are performed in vacuum [4,5,7], humid atmosphere [1], or liquid [2,3,8] to study the damaging mechanisms and their efficiency. The broad range of experimental setups is owed to the different scattering properties of the diverse radiation types [1,3,8,9] and various production channels of secondary scattering products. The macroscopic results depend strongly on the specific experimental setup, the type of radiation, and the concentrations of species used. This makes it difficult to quantitatively compare results of different studies. To overcome this problem, we propose a combined experimental and simulational approach to determine microscopic damage-dose relationships which are independent of the macroscopic experimental details. Thereby, the experimental geometry is modeled, the particle scattering events and energy deposits are simulated, and the microscopic energy deposit per target molecule is calculated. This can be performed for arbitrary radiation sources and experimental geometries and makes results from different series of measurement quantitatively comparable. To investigate the damage dependence on different radiation track structures, the resulting energy deposit, the spatial distribution of events, secondary scattering products, particle mean free paths, or the fluency of particles have to be properly taken into account [10,11]. This results in better comparable data and concomitantly in better understanding of the underlying molecular processes. In the following the general approach and procedure are explained and afterwards applied to the electron irradiation of plasmid DNA in liquid. This example was chosen to demonstrate the usefulness of our approach, even in the case of a system with very inhomogeneous energy deposit, such as those resulting from irradiation of DNA in water with keV electrons.

*hahn@physik.fu-berlin.de
†tihomir.solomun@bam.de

II. GENERAL APPROACH

When molecules are irradiated, the damage is measured in dependence of the exposure to external radiation. Yet,

to make the results generally comparable, the damage has to be expressed in dependence of the microscopic events which are suspected to cause the damage [11]. This may be events such as the energy deposit within the molecule and its surroundings, or the production of secondary particles which may act as damaging agents. From an experimental point of view, it is very challenging to measure properties such as the energy deposit in a micrometer subvolume of a liquid. However, thanks to the availability of Monte Carlo codes, such as GEANT4, the track structure and scattering events can be simulated for all naturally occurring particles and materials [12,13]. This makes it possible to model experimental setups and to calculate particle tracks, energy deposit, scattering events, and production of secondary particles with nanometer resolution [14]. Thereby, it has to be taken care that all relevant scattering processes for the particles involved (e.g., photons, electrons, nucleons, and ions) are supported and activated in the simulation and that they are validated in the energy range of interest [12,13]. For an overview of supported particles and scattering processes we refer to Agostinelli *et al.* [12] and Incerti *et al.* [13] and the references therein. The simulation results can be used to calculate the events occurring at a certain molecule at a specific position. In the following a simulated energy deposit per volume element and per primary particle at position r is denoted as $E_{\mathrm{sim}}(r)$.

Since the biologically relevant processes are happening in water, experiments have to be performed under similar conditions to incorporate water mediated damaging processes [15]. In a liquid medium, diffusion or convection can lead to molecule displacement during the irradiation. In general, this displacement can be calculated under the consideration of the specific experimental geometry, temperature flux, and molecular mobility. The resulting trajectory for the kth time step is represented in the following by r_k. These trajectories can be convoluted with the spatially resolved information about the energy deposit $E_{\mathrm{sim}}(r)$ by inelastic scattering events to obtain the total energy deposit at the target upon irradiation. Therefore, a target volume has to be assigned to each molecule or cell. Within this target volume an energy deposit is assumed to have a certain probability to damage the target. The dimension of the target volumes depends on the object and interaction of interest [11]. In the case of direct damage to a molecule the target volume is usually assumed to consist of the molecular volume including the first hydration shell [16]. To include indirect effects the target volume has to be extended to additional water layers, from within which secondary particles are assumed to reach the target. In the study of cells and bystander effects the target volume has to include even more than one cell [11]. After defining an appropriate target volume (V), a summation over all energy densities $E_{\mathrm{sim}}(r_k)$ can be performed to calculate the total energy deposit $[E(V)]$ within the target. Furthermore, E has to be normalized to the number of time steps in the diffusion and convection simulations (τ), which is the ratio of the experimental irradiation time (t_{expt}) and the time step of the simulation (t_{sim}): $\tau = t_{\mathrm{expt}}/t_{\mathrm{sim}}$. Then the sum of the total energy deposit into a target with volume V becomes

$$E(V) = \sum_{k}^{\tau} \frac{E_{\mathrm{sim}}(r_k)\, V}{\tau}. \tag{1}$$

Scattering experiments with particles whose elastic mean free paths in the liquid are much smaller than the geometric dimensions of the sample holder result in a spatially inhomogeneous distribution of the events. Therefore, the convolution of the particle positions with such an inhomogeneous event distribution leads to a broad, unsymmetrical distribution of particles experiencing each a certain number of events. The experimental data for the undamaged species (S, survival rate) in dependence of the number of primary particles (x) is equal to the sum over the number of irradiated species (N_i) which experienced each the same amount of energy deposit or events $[E_i(V)]$ as determined by Eq. (1) and summation index i. The assumed damage-energy or damage-event relation $f(x, E_i(V))$ of the measured survival rate has to be represented by an adequate model (e.g., linear-quadratic model, target theory) [10,17,18]:

$$S = \sum_{i=0} N_i\, f(x, E_i(V)). \tag{2}$$

This model can be tested by fitting Eq. (2) to the experimental data. Such an obtained energy- or event-damage relationship has the advantage of being independent of external parameters. This is achieved by absorbing the experimental conditions in the parameters E_i and N_i as described above. Therefore, the results analyzed by this procedure permit a correct comparison of the data obtained by different experimental approaches. An example for this is given in the following section.

III. APPLICATION TO ELECTRON IRRADIATION OF DNA IN WATER

In the presented experiment, plasmid DNA (pUC19) in water was directly irradiated with electrons. The electron trajectories, the inelastic scattering events, and the resulting energy deposit within water were simulated. Afterwards the randomly chosen plasmid locations were convoluted with the energy deposit. This is schematically sketched in Fig. 1. In combination with the experimental results and a damaging model based on the target theory [17] the event-damage

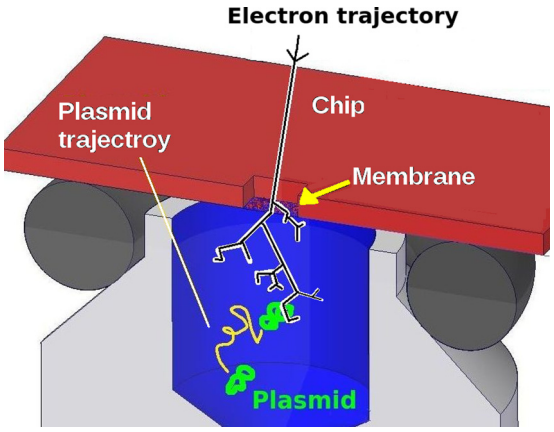

FIG. 1. Sketch of the setup for electron irradiation of plasmid DNA in liquid. The plasmids diffuse on a random trajectory through the liquid. During this diffusion plasmids cross the trajectory of the electrons which are scattered at the membrane in the center of the chip and in water.

relation was calculated. Here, the event-damage relation was expressed as a decrease of undamaged plasmids in dependence of the microscopic energy deposit in the target volume. In the following this is explained and discussed in detail.

A. Experimental section

The plasmid DNA (pUC19 with 2686 base pairs and a mass of 2.9×10^{-21} kg) was isolated with QlAprep Spin Miniprep Kit (Qiagen) from *Escherichia coli* Top10 and eluated with ultrapure water (conductance 0.055 μS cm^{-1}). A volume of 4 μL with a plasmid concentration of 50 ng μL^{-1} in ultrapure water was used for irradiation. The sample was placed in our custom made sample holder incorporating a 100-nm-thick silicon nitride membrane with an additional layer of 10-nm-thick silicon dioxide. The membrane is nearly transparent for electrons of 30 keV (transmission about 92% [8]) and withstands pressure differences of up to 1 bar. This makes it possible to irradiate the enclosed liquid samples within a vacuum environment by electrons as sketched in Fig. 1. The experimental setup was extensively described in our previous work [8]. The irradiation experiments were performed within a FEI XL30 scanning electron microscope (SEM) equipped with a LaB_6 cathode. The irradiation was performed for 300 ± 2 s with a primary electron energy of 30 keV, SE-detector voltage 0 V, and a pressure below 1×10^{-6} mbar. For the irradiation a SEM scan size of 350×266 μm^2 was chosen. Before and after irradiation, the electron current was measured at a Faraday cup with a picoammeter (Keithley 6485). After irradiation the samples were analyzed by means of gel electrophoresis (50 ng per lane, 100 V, 40 min, 1% agarose gel, and GelRed) and intensity profiles were extracted. A linear background subtraction and a Gaussian multipeak fit was performed using the FITYK software [19] with a Levenberg-Marquardt algorithm.

The undamaged plasmid exists in a topological constrained form, that is, supercoiled. When a single-strand break (SSB) or multiple SSBs occur, energy gets released and it relaxes to an open circular form. In case of a double-strand break (DSB) it relaxes from the open circular form to a linear conformation. These three forms, supercoiled (undamaged), circular (SSB), and linear (DSB), can be separated due to their different electrophoretic mobility within the gel. The results were normalized to the total intensity of the respective gel lane.

B. Theoretical section

The goal of the simulations is to calculate the microscopic event and energy distribution of the plasmids upon irradiation from the experimental parameters such as the number of primary electrons, their kinetic energy, the membrane thickness, sample holder geometry, plasmid volume, and their movement. During the irradiation, the plasmids move through the liquid while encountering primary electrons and secondary particles (Fig. 1). The number of scattering processes which occur in their vicinity and the energy deposited nearby depend strongly on their location and the local electron flux. To determine both quantities, electron-scattering simulations and calculations regarding the plasmid movement were performed as described below. The convolution of the plasmid location with the spatially resolved energy deposit results in the microscopic event and energy distribution for the plasmids as shown further below.

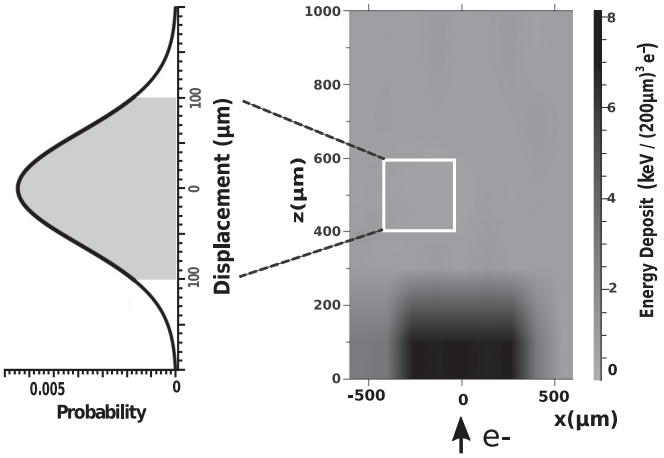

FIG. 2. Right: False color representation of the energy deposit behind the membrane projected on the x-z plane. The square represents a region of 200×200 μm^2. Left: For the irradiation time of 300 s, 90% of the plasmids remain within the square as displayed on the left side and indicated by the gray area under the Gaussian distribution. For details see the text.

1. *Electron-scattering simulations*

To obtain the spatially resolved events and energy deposits within the liquid, Monte Carlo simulations (MCSs) of the scattering processes were performed. Thereby, the GEANT4 MCS framework (10.02) [12] was used to simulate the 30 keV electron beam scattering at the 100-nm Si_3N_4 membrane, the 10-nm SiO_2 layer, and the liquid volume. Within the membrane the G4EmPenelope models [20] were applied. More specifically, an electron beam (10^8 electrons) with momentum vector perpendicular to the membrane surface was simulated. The starting positions were chosen randomly within the scan size (350×266 μm^2) of the SEM used in the experiment. In the liquid volume the optimized DNA extension [13] for interaction of low energy particles with water was used. The following processes for electron-water interaction were activated, with the implementations given in parentheses: elastic scattering (Champion elastic model), ionization (Born ionization model), electronic excitation (Born excitation model), electron attachment (Melton attachment model), and vibrational excitation (Sanche excitation model). From the simulations the occurrence of these inelastic scattering events and the energy deposit per volume element and primary electron was extracted. The projection of the energy deposit on the x-z plane is sketched in Fig. 2. There, the highest energy deposit is found in the region behind the membrane, while it decreases until the end of the sample holder at depth of 1 mm and to its edges. Furthermore, the kinetic energy distribution of the electrons was calculated for selected depths in water and a bin size of 10 eV as shown in Fig. 3. For better comparability the values are normalized with respect to the total number of electrons with kinetic energies below 200 eV at 100 μm water depth. The percentage of

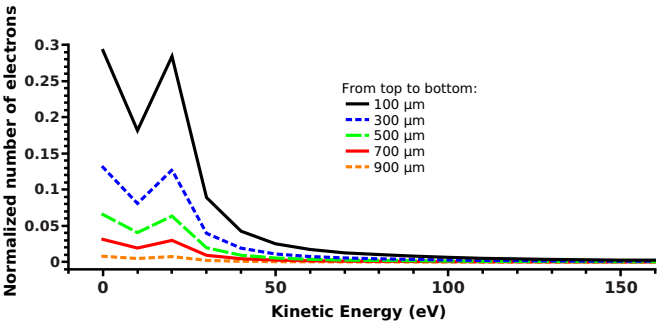

FIG. 3. Simulated kinetic energy distribution of the electrons at various water depths behind the membrane with a bin size of 10 eV. From top to bottom: 100 μm (black line), 300 μm (blue dots), 500 μm (broken green line), 700 μm (red line), and 900 μm (orange dots). All curves were normalized to the total number of electrons at 100 μm depth.

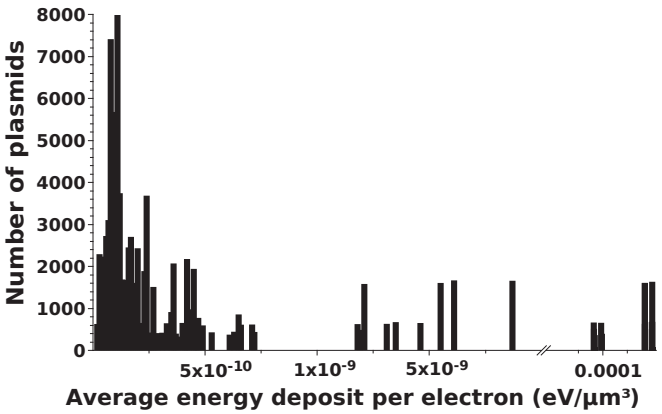

FIG. 4. Number of plasmids for various energy deposits per primary electron per 1 μm^3. Calculations were performed for 10^5 plasmids and a bin size of 10^{-11} eV. Most of the plasmids reside in regions where the energy deposit is below 5×10^{-10} eV μm^{-3} per primary electron.

electrons having energies between 0 and 10 eV is about 30%, between 10 and 20 eV is 18%, and between 20 and 200eV is 52%. The total number of electrons decreased with depth in the water while the relative kinetic energy distribution of the electrons between 100 and 1000 μm did not change significantly (Fig. 3). The relative amounts of the inelastic electron-water scattering events are as follows: ionization (79%, 446 per primary electron), vibrational excitation (19%, 105), electronic excitation (2%, 13), and electron attachment (<1%, less than one per primary electron). The dominance of the ionization interactions is due to the fact that most of the secondary electrons have kinetic energies above 20 eV where the ionization cross section predominates [21].

2. *Diffusion and convection*

To describe the plasmid movement during the irradiation, directed convection and random diffusion have to be considered. As a critical phenomenon convection appears in a liquid between two plates when the product γ of the Grashof number (Gr) and Prandtl number (Pr) is equal to $\gamma = 67.4$ [22]:

$$\gamma = \mathrm{PrGr} = \frac{AR^4 g\beta}{\chi \nu}, \tag{3}$$

with the temperature gradient A, the cylinder radius R, the gravitational acceleration g, the thermal expansion coefficient β, the thermal diffusivity χ, and the viscosity ν of water. Assuming that the temperature gradient originates from the heating induced by the electron current (10^{12} electrons with 30 keV) within a water layer of 12.5 μm, where according to our simulations over 99% of the energy is deposited [8], with cylindrical geometry and a radius of the sample container of 0.8 mm [8], Eq. (3) results in $\gamma = 0.53$, being much smaller than the critical value of 67.4. Therefore, it can be concluded that within our setup the plasmid movement is purely governed by diffusion without contributions from convection. The average displacement due to diffusion in one dimension (λ) is given by the following equation [23]:

$$\lambda = \sqrt{2\delta t}. \tag{4}$$

With the diffusion constant $\delta = 6.38$ μm^2 s^{-1} [8] at 303 K and an irradiation time of 300 s, the average displacement becomes 61.9 μm. Thus after 300 s on average 90% of the plasmids are located within a cube with an edge length of 200 μm as visualized on the left side of Fig. 2 by the Gaussian and the gray area corresponding to 90% probability. Hence we can average the energy deposit over cubic subvolumes with 200 μm edge length instead of simulating a random walk through our sample holder geometry. Otherwise, the necessity to simulate over 10^{10} primary electrons to obtain a spatially dense energy deposit with a micrometer granularity would result in high computational cost [24] without increasing the accuracy of our predictions much. By assuming an equal distribution of the plasmids throughout these subvolumes an energy deposit histogram of the plasmids can be obtained by Eq. (1) with $\tau = 1$ and the target volume V. The resulting histogram is displayed in Fig. 4 and shows the distribution of the plasmids (N_i) with respect to the direct energy deposit (E_i) within 1 μm^3 per primary electron. The median of the distribution is 1.7×10^{-10} eV μm^{-3} per electron and the mean 3.5×10^{-5} eV μm^{-3} per electron.

3. *The target volume*

The goal of this section is to estimate the target volume in which an energy deposit can lead to a single- or double-strand break in undamaged plasmids. In general these strand breaks are assumed to occur at the sugar-phosphate backbone connecting the nucleobases within one strand of the DNA molecule [25]. For supercoiled and circular plasmids the number of the sugar-phosphate backbones is twice the number of base pairs (bp). Therefore, there are 2×2686 sensitive subvolumes within one pUC19 plasmid, where damage can lead to a SSB or DSB. Hence, the critical task is to obtain the dimensions of these subvolumes. Various studies [18,26–28] investigated the energy deposit in cylindrical and spherical subvolumes with characteristic length up to 100 nm. Lindborg *et al.* [18,28] found that for subvolumes with 10–15 nm diameter the dose mean lineal energy ($\bar{y}_D$) is proportional

to the α value of the linear-quadratic relationship [18] used in clinical radiation therapy for low and high Linear energy transfer (LET) radiation. This was deduced from an analysis of clinical values for the radiobiological effectiveness ($W_{\mathrm{iso}E}$) [29] and $\bar{y}_D$ [18]. Thereby, the linear-quadratic relation was applied with the biological effect (BE) of n irradiations of dose (D) and the dose coefficients α and β: $\mathrm{BE} = \alpha n D + \beta n D^2$. This corresponds in the simplified case for $n = 1$ and $\beta = 0$ to the single-hit model used in the following section [Eq. (6)] and is valid due to the absence of the repair or other complex processes in pure plasmid DNA as compared to the biological tissue as studied by Lindborg *et al.* [18]. Therefore, one can assume that the energy deposit within a sphere of 15 nm diameter is of biological relevance. From these considerations, it is assumed that the target volume of a plasmid can be modeled as the sum of the subvolumes. Thereby, the overlap of the spheres is counted for each sphere individually in the total target volume. This is because an energy deposit within the overlapping region increases the probability of a strand break in both sensitive volumes whereby one SSB is sufficient to count as damage. Hence the target volume (V) can be written as

$$V = 2bp\frac{4}{3}\pi\left(\frac{d}{2}\right)^3 = 7.12 \times 10^6\ \mathrm{nm}^3 \tag{5}$$

with the number of base pairs (bp = 2686) and the diameter ($d = 15$ nm) of the sphere representing the sensitive subvolume. This target volume (7×10^6 nm^3) including the indirect effects of radiation is three orders of magnitude bigger than the volume of the plasmid including the first hydration layer ($V_{\mathrm{pUC19}} = 6.12 \times 10^3$ nm^3), which is used to calculate the direct effects of radiation [8]. Here it has to be noted that on the microscopic scale the energy is not smoothly deposited over the irradiated volume. It is distributed along the tracks of the primary particles whose stochastic interactions with the traversed medium lead to an inhomogeneous event distribution [11]. Therefore, the average deposited energy in the whole target volume may be even deposited only in one of the subvolumes representing the sugar-phosphate backbone.

In an ideal situation one could follow each particle and its secondary scattering products individually and analyze their energy deposit in space and time. Still, with the currently available computational resources it is not practicable to calculate 10^{12} primary electron trajectories in a macroscopic volume in a reasonable time. Hence, to obtain a measure for the energy deposit $E(V)$ at the plasmid [Eq. (1)] we set the averaged energy deposit at the plasmid locations [$E_{\mathrm{sim}}(r_k)$ in cubes of (200 μm)^3 as discussed in the diffusion section] in relation to the target volume [compare Eq. (1)]. This energy deposit can be connected by an appropriate damage model to the experimental data to obtain the damage-dose relation as stated in Eq. (2).

4. The damage model

In standard irradiation studies all members of the irradiated species are assumed to receive on average the same dose. In order to evaluate the dose-damage relation for biomolecules a single-target single-hit model [10,17] can be fitted to the experimental data:

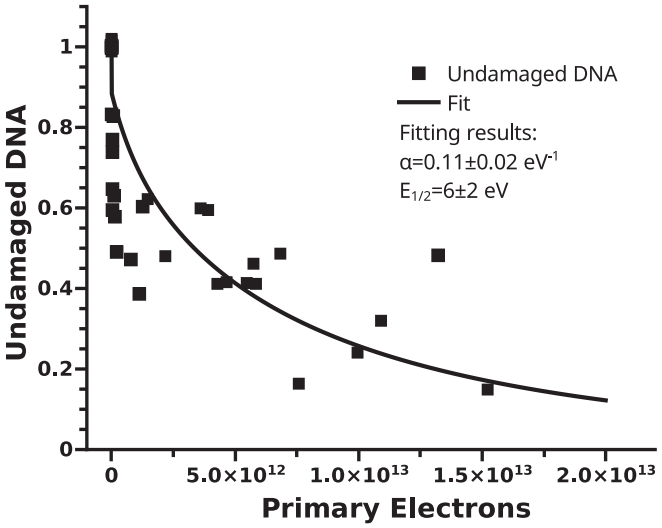

FIG. 5. Change in the number of undamaged plasmids in dependence of the amount of primary electrons with 30 keV incident energy. The curve is a fit according to Eq. (7).

$$S = e^{-\alpha E}. \tag{6}$$

Thereby, S is the survival rate (relative amount of undamaged species), α the fitting parameter (dose coefficient), and E the deposited energy. In contrast to standard irradiation experiments the species irradiated within the presented experiment received a broad asymmetric distribution of energy deposits as determined by the simulation and displayed in Fig. 4. Therefore, the applied target-hit model has to be modified to incorporate the various doses. The measured survival rate S in dependence of external dose (Fig. 5) consists of the survival rate S_i weighted by the number of plasmids, N_i, and their respective energy deposit E_i. By assumption that all S_i obey the single-hit model [17] (exclusion of nonlinear effects), the dose coefficient α is independent of the energy deposit E_i. Hence, the measured survival rate (S) can be written as the sum of the calculated survival rates (S_i) obeying all the same dose-damage relations with the same dose coefficient. Together with Eq. (2), where $f(x, E_i(V)) = e^{-\alpha x E_i(V)}$, this results in the following dose-damage model:

$$S = \sum_{i=0} S_i = \sum_{i=0} N_i e^{-\alpha x E_i(V)}. \tag{7}$$

This makes it possible to perform a single parameter fit for α even for the situation of varying energy deposits E_i over the sample geometry. Thereby, S is the experimental determined survival rate and x the amount of primary electrons. N_i represents the relative number of plasmids receiving a certain energy deposit E_i per primary electron as determined by the MCS and displayed in Fig. 4. The results are shown in Fig. 5. Part of the data above 5×10^{12} primary electrons having the same irradiation time (300 s) originates from our previous work [8]. The fit leads to $\alpha = 0.11 \pm 0.02$ eV^{-1}, a median lethal energy deposit of $E_{1/2} = 6 \pm 2$ eV (50% undamaged plasmids), and the corresponding value for $E_{1/10} = 18 \pm 4$ eV (10% undamaged plasmids). The uncer-

tainty is calculated by the fitting algorithm (PYTHON SCIPY 0.13.3).

IV. RESULTS

In the first section we presented a general approach to derive the local energy deposit at biological targets after irradiation. The results become independent of the experimental details such as sample geometry or radiation type. More specifically, the combination of particle-scattering simulations, calculations concerning the trajectory of the target, and sample holder geometry were described. From this, the parameter of microscopic dose-damage models can be calculated and compared for various experimental conditions. In the second part, the application of this approach to the electron irradiation of DNA in water was demonstrated. By simulation of electron scattering the spatially resolved energy deposit over the whole solution was determined. Under the experimental condition of this work, the scattering events were found to take place over the whole sample, with the preponderant part of the energy deposit taking place in a narrow volume directly behind the membrane (Fig. 2). In addition, the plasmid movement due to convection and diffusion was calculated. Based on hydrodynamic considerations, convection due to the electron-beam-induced heating was ruled out. From the calculation of the diffusional movement of the plasmids, it was calculated that over 90% stay within a box of 200-μm edge length. The determination of the target volume for the induction of strand breaks is based on the work of Lindborg *et al.* [18]. Thereby, a subvolume of 15 nm diameter around each sugar-phosphate backbone is assumed in order to calculate the total target volume ($V = 7.12 \times 10^6$ nm^3) of the plasmid. This volume includes the processes which lead to direct and indirect DNA damage. In combination with an extended single-hit single-target model [Eq. (7)] a median lethal energy deposit of $E_{1/2}^{\text{total}} = 6 \pm 2$ eV and the corresponding $E_{1/10}^{\text{total}} = 18 \pm 4$ eV was determined. The value for the direct damage ($V_{\text{pUC19}} = 6.12 \times 10^3$ nm^3) is calculated as $E_{1/2}^{\text{direct}} = 0.05 \pm 0.02$ eV.

V. DISCUSSION

Before interpreting the radiation biological consequences and underlying physical mechanisms of the results, we discuss their dependence on the various experimental and simulation parameters. First of all, the uncertainty of the dose coefficient was found to be 19% as determined by the fit of Eq. (7) to the experimental data (Fig. 5). The energy deposit within the sample holder was determined by electron-scattering simulations and estimations about the plasmid diffusion. These results depend on the scattering cross sections for the electron-water interactions within the GEANT4 DNA framework which are based on extrapolations of water vapor data to the liquid or ice [13]. The uncertainty in the cross section is largest for the interaction of low energy electrons (LEE, $E_{\text{kin}} < 100$ eV). Since these species have a mean free path length in liquid water in the nanometer range and the energy averaging in this study is performed over 200 μm, these uncertainties are, however, of minor influence. The value with the highest uncertainty is the target volume V which has a cubic dependence on the diameter [Eq. (5)]. This is due to the fact that the diameter

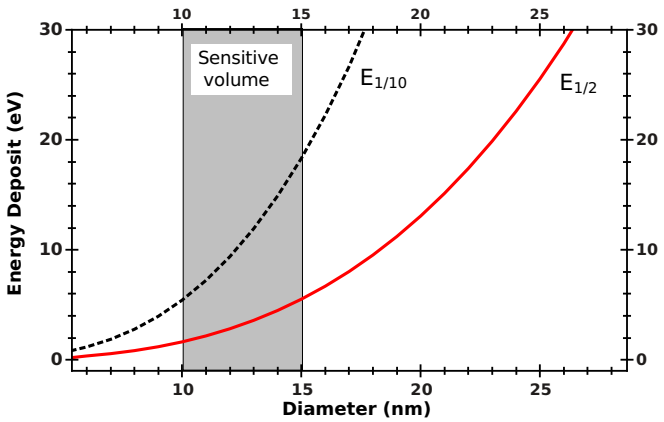

FIG. 6. The energy deposit in dependence of the diameter of the sensitive subvolume around the sugar-phosphate backbone as result of the fit of Eq. (2) for various volumes [Eq. (5)] in dependence on the diameter. The broken black ($E_{1/10}$) and red ($E_{1/2}$) lines represent the average energy deposit within a plasmid volume required to damage 90% and 50% of the plasmids, respectively. The gray shaded region represents the biological sensitive diameter of 10–15 nm according to Lindborg *et al.* [18]. For details see the text.

was deduced by Lindborg *et al.* [18] from a comparison of the α ratio and dose mean-lineal energy ratio for five types of radiation. Thereby, the simulated and measured data taken from various studies have uncertainties around 20%. For the reference radiation, a ^{60}Co γ-therapy beam, an uncertainty of 15% was given. From the resulting uncertainty of the diameter follows an uncertainty of the volume and the median lethal energy of 60% [Eq. (5)]. Therefore, our results have to be given as follows: $E_{1/2}^{\text{total}} = 6 \pm 4$ eV and the corresponding $E_{1/10}^{\text{total}} = 18 \pm 11$ eV. To visualize the influence of this systematic uncertainty of the target volume we fitted Eq. (5) for diameters of the sensitive subvolume between 5 and 30 nm and displayed the results for $E_{1/2}$ and $E_{1/10}$ in Fig. 6. The relation between diameter and target volume is given by Eq. (5). Thereby, the highlighted region represents the values within the diameter range given by Lindborg *et al.* [18]. One can easily see in Fig. 6 how small changes in diameter lead to large changes in the calculated energy deposit. To decrease the uncertainty of the diameter, its recalculation based on an increased number of clinical studies with more radiation types and broader energy ranges would be very beneficial.

To put these results into context one has to consider the energy thresholds for direct and indirect damaging processes. Most of the purely simulational studies assume critical energies of 10–17 eV for direct SSB induction by means of energy deposit in the sugar-phosphate backbone [11,25,30]. From vacuum studies it is known that even photons with energies (7 eV) below the DNA ionization threshold (9 eV) can damage DNA via direct absorption [31]. Similar vacuum experiments with electrons found damage induction in DNA even below 7 eV [21]. This damage was attributed to resonant processes [32] such as dissociative electron attachment (DEA) [5]. Although our median lethal energies are in this range (6 ± 4 eV), one has to consider that the direct energy deposit within DNA is only about 1% in comparison with the given target volume. The indirect effects are due to the energy deposit

in the sensitive subvolume near the sugar-phosphate backbone and the production of reactive species as discussed below. On a nanometer scale, the energy deposit over the target volume is nonhomogeneously distributed due to the stochastic nature of the scattering process [11]. This fact can be used to estimate the average number of sensitive subvolumes where energy gets deposited. Therefore, we consider the minimal energies of the characteristic electron-water scattering processes as included in the MCS. The production of "kinetic" ($E > 0$ eV) secondary electrons by ionization takes place above 10 eV [13]. Electronic excitations in water are simulated from 9 eV; the energy range of an electron-water attachment is between 4 and 13 eV [13]. From the scattering simulation we know that over 90% of all inelastic processes (excluding vibrations) are ionizations with an energy threshold at 11 eV. This is due to the average kinetic energy of the electrons of around 30 eV and the fact that ionization is the dominant scattering process above 15 eV [21,33]. Below 15 eV the resonant processes [34] become dominant, namely DEA for $E > 0$ [5,6,21] and dissociative electron transfer (DET) for $E < 0$ [2,35]. Nevertheless, we can state so far that the majority of secondaries produced are generated via ionization. In the case of the median lethal energy deposit of 6 ± 4 eV, which corresponds to on average one SSB per 12-eV energy deposit, it follows from the involved energy threshold for ionization processes that on average less than two ionizations in the sensitive subvolume lead to at least one SSB. This is in accordance with the MCS performed by Nikjoo *et al.* [25] for damage dependence on ionization events in the surrounding of DNA. Further simulational work by Friedland *et al.* [30] is also compatible with our determined median lethal energy deposit. They found the best agreement for simulated SSB yields with the experimental data for an energy threshold of 9.5 eV around DNA, which was represented by detailed chromatin fiber models. From the low energy values and the low number of necessary ionization events to cause a SSB, the secondaries produced within the sensitive subvolume can be assumed to have a high likelihood to induce strand breaks. These secondaries are produced for the most part via ionization of water, which can be described by the following net ionization reaction [1,36]:

$$e^- + 2H_2O \rightarrow H_3O^+ + OH^\bullet + e'^- + e_2^-. \qquad (8)$$

Thereby, the OH radical [37], the LEE [1], and its successor, the prehydrated electron [2], are the most lethal agents. The average ranges these species can access before they react with the aqueous surroundings are on the order of nanometers: The LEE penetration length in liquid water at 298 K was reported to be 0.4–20 nm [38–40]. Thereby, in the energy range 7–20 eV the maximum values are around 20 nm, decreasing in the subexcitation energy range (<7.3 eV) with a mean of 8.8 nm [38]. The prehydrated electron with a lifetime of a few hundred femtoseconds has an initial delocalization length of about 4 nm [41]. Values of the OH-radical diffusion length are in the range 2–7 nm and depend on the diffusion constant ($\delta_{OH} = 2.8\ nm^2\ s^{-1}$) and scavenging capability of the surrounding medium [36,42,43]. These ranges on the order of nanometers make it plausible that the radius of the sensitive subvolume of 7.5 nm, as determined by Lindborg *et al.* [18], is of biological relevance. A more detailed analysis has to include the interplay of ionization events and the diffusional behavior of the various secondary species near the sugar-phosphate backbone, by directly simulating the chemical stage [44]. This possibility was recently introduced into GEANT4 [36,44] and will be applied in future work. Thereby, detailed diffusion models for plasmids and secondary products and their reaction kinetics should be considered, taking into account microscopic attachment probabilities to different DNA sites, production rates, their lifetimes, and plasmid structures [30,36].

VI. CONCLUSION

In this work we have presented a general method to determine the energy deposit in the biologically relevant target volume of biomolecules independent of the experimental setups. Its derivation was motivated by the need to compare experimentally obtained energy-damage relations independent of the specific experimental details such as sample geometry or the type of primary radiation.

The convolution of the spatially resolved energy deposit is determined by the particle-scattering simulations. The energy deposit is convoluted with the trajectories of the biomolecules. As a result, the number of biomolecules experiencing a certain energy deposit is obtained. This distribution is used to determine the relation between the microscopic energy deposit and the experimentally determined damage.

The method was applied to the direct electron irradiation of DNA in water. Here a sensitive subvolume around the sugar-phosphate backbone with a diameter of 15 nm was chosen based on the work of Lindborg *et al.*

In accordance with radiation chemistry, we found that most of the damage has to be attributed to indirect damage caused by energy deposit in the sensitive subvolume. The direct energy deposit of about 1% was comparatively small: $E_{1/2}^{\text{direct}} = 0.05 \pm 0.02$ eV. The median lethal energy including indirect effects was determined as $E_{1/2}^{\text{total}} = 6 \pm 4$ eV and the value for 90% damaged DNA as $E_{1/10}^{\text{total}} = 18 \pm 11$ eV. The huge uncertainty of 60% is owed to the cubic dependence on the diameter as given by Lindborg *et al.* [18,28]. To achieve a higher accuracy, further work has to be dedicated to decrease the uncertainty of the diameter of the sensitive subvolume. By considering the characteristic interaction energies for electron-water scattering, we found that on average less than two ionizations in the sensitive subvolume lead to at least one SSB. This is in agreement with the calculations of Nikjoo *et al.* [25] and shows the high efficiency of secondary products of radiation-water interaction in damaging DNA.

The presented method can be applied to the quantitative study of all kind of radiation, such as photons and electrons, and their effects on biomolecules or even cells under various conditions, such as different pH or salinity. This allows for a better understanding and comparability of the damaging effects of microscopic energy deposit as it can be obtained by microdosimetry calculations. In principle, our method can be extended to the study of nucleons or ions [9,45]. Here it has to be taken care that the cross section for nuclear interactions between the atoms of the biomolecule and H_2O can differ such that the direct damage can be enhanced. This can be included in the presented method by simulating two

targets, the biomolecule with its specific atomic composition and the surrounding water. We leave the detailed discussion of this extension to future studies. Furthermore, our method can be extended to include the simulation of the so-called chemical stage [44] and the indirect effects of OH radicals, prehydrated electrons, and ions. This makes it possible to extend the interpretation of real-world experiments from the classic dosimetric description of biologically relevant molecular damage in dependence of energy deposit, to the dependence on events, induced by the secondary radiation products [11,46] or even the combination of fluence and mean free path as proposed by Simmons and Watt [10].

ACKNOWLEDGMENT

This work was supported by the German Science Foundation (DFG) under Contract No. STU 245/4-1.

[1] E. Alizadeh, A. G. Sanz, G. Garcia, and L. Sanche, J. Phys. Chem. Lett. **4**, 820 (2013).
[2] J. Nguyen, Y. Ma, T. Luo, R. G. Bristow, D. A. Jaffray, and Q.-B. Lu, Proc. Natl. Acad. Sci. USA **108**, 11778 (2011).
[3] J. S. D'Souza, J. A. Dharmadhikari, A. K. Dharmadhikari, B. J. Rao, and D. Mathur, Phys. Rev. Lett. **106**, 118101 (2011).
[4] M. Folkard, K. Prise, B. Vojnovic, S. Davies, M. Roper, and B. Michael, Int. J. Radiat. Biol. **64**, 651 (1993).
[5] X. Pan, P. Cloutier, D. Hunting, and L. Sanche, Phys. Rev. Lett. **90**, 208102 (2003).
[6] S. Ptasińska and L. Sanche, Phys. Rev. E **75**, 031915 (2007).
[7] T. Solomun, H. Seitz, and H. Sturm, J. Phys. Chem. B **113**, 11557 (2009).
[8] M. B. Hahn, S. Meyer, M.-A. Schröter, H. Seitz, H.-J. Kunte, T. Solomun, and H. Sturm, Phys. Chem. Chem. Phys. **19**, 1798 (2017).
[9] A. V. Solov'yov, E. Surdutovich, E. Scifoni, I. Mishustin, and W. Greiner, Phys. Rev. E **79**, 011909 (2009).
[10] J. A. Simmons and D. E. Watt, *Radiation Protection Dosimetry: A Radical Reappraisal* (Medical Physics Publishing, Madison, WI, 1999).
[11] D. T. Goodhead, Radiat. Prot. Dosim. **122**, 3 (2006).
[12] S. Agostinelli *et al.*, Nucl. Instrum. Methods Phys. Res. Sect. A **506**, 250 (2003).
[13] S. Incerti *et al.*, Med. Phys. **37**, 4692 (2010).
[14] M. A. Bernal *et al.*, Phys. Med. **31**, 861 (2015).
[15] E. Alizadeh, T. M. Orlando, and L. Sanche, Annu. Rev. Phys. Chem. **66**, 379 (2015).
[16] H. Nikjoo, D. T. Goodhead, P. O'Neill, and P. Terrissol, Int. J. Radiat. Biol. **71**, 467 (1997).
[17] D. E. Lea, *Actions of Radiations on Living Cells*, 2nd ed. (Cambridge University Press, Cambridge, U.K., 1962).
[18] L. Lindborg, M. Hultqvist, Å. C. Tedgren, and H. Nikjoo, Phys. Med. Biol. **58**, 3089 (2013).
[19] M. Wojdyr, J. Appl. Crystallogr. **43**, 1126 (2010).
[20] M. Vilches, S. García-Pareja, R. Guerrero, M. Anguiano, and A. M. Lallena, Nucl. Instrum. Methods Phys. Res. Sect. B **254**, 219 (2007).
[21] E. Alizadeh and L. Sanche, Chem. Rev. **112**, 5578 (2012).
[22] L. D. Landau, E. M. Lifschitz, P. Ziesche, and W. Weller, *Hydrodynamik*, 4th ed., Lehrbuch der Theoretischen Physik, Vol. 6 (Akademie Verlag, Berlin, 1981).
[23] A. Einstein, Ann. Phys. **322**, 549 (1905).
[24] Resulting in an estimated computing time of more than a year on a recent HPC system with 24 cores and 64 GB RAM.
[25] H. Nikjoo, R. F. Martin, D. E. Charlton, M. Terrissol, S. Kandaiya, and P. Lobachevsky, Acta Oncol. **35**, 849 (1996).
[26] H. Nikjoo, D. T. Goodhead, D. E. Charlton, and H. G. Paretzke, Int. J. Radiat. Biol. **60**, 739 (1991).
[27] B. Grosswendt, Radiat. Prot. Dosim. **122**, 404 (2006).
[28] L. Lindborg, M. Hultqvist, Å. C. Tedgren, and H. Nikjoo, Radiat. Prot. Dosim. **166**, 339 (2015).
[29] *Relative Biological Effectiveness in Ion Beam Therapy*, Technical Report Series No. 461 (International Atomic Energy Agency, Vienna, 2008), pp. 1–153.
[30] W. Friedland, P. Jacob, H. G. Paretzke, and T. Stork, Radiat. Res. **150**, 170 (1998).
[31] K. Prise, I. Munro, M. Folkard, B. D. Michael, B. Vojnovic, B. Brocklehurst, and A. Hopkirk, Int. J. Radiat. Biol. **76**, 881 (2000).
[32] J. Simons, Acc. Chem. Res. **39**, 772 (2006).
[33] M. A. Huels, B. Boudaïffa, P. Cloutier, D. Hunting, and L. Sanche, J. Am. Chem. Soc. **125**, 4467 (2003).
[34] T. M. Orlando, D. Oh, Y. Chen, and A. B. Aleksandrov, J. Chem. Phys. **128**, 195102 (2008).
[35] C.-R. Wang, J. Nguyen, and Q.-B. Lu, J. Am. Chem. Soc. **131**, 11320 (2009).
[36] M. S. Kreipl, W. Friedland, and H. G. Paretzke, Radiat. Environ. Biophys. **48**, 11 (2008).
[37] C. von Sonntag, *Free-Radical-Induced DNA Damage and Its Repair* (Springer, Berlin, 2006).
[38] J. Meesungnoen, J.-P. Jay-Gerin, A. Filali-Mouhim, and S. Mankhetkorn, Radiat. Res. **158**, 657 (2002).
[39] S. Uehara and H. Nikjoo, J. Radiat. Res. **47**, 69 (2006).
[40] H. Nikjoo and L. Lindborg, Phys. Med. Biol. **55**, R65 (2010).
[41] J. Savolainen, F. Uhlig, S. Ahmed, P. Hamm, and P. Jungwirth, Nat. Chem. **6**, 697 (2014).
[42] R. Roots and S. Okada, Radiat. Res. **64**, 306 (1975).
[43] J. F. Ward, Int. J. Radiat. Biol. **57**, 1141 (1990).
[44] M. Karamitros *et al.*, J. Comput. Phys. **274**, 841 (2014).
[45] T. T. Böhlen, F. Cerutti, M. Dosanjh, A. Ferrari, I. Gudowska, A. Mairani, and J. M. Quesada, Phys. Med. Biol. **55**, 5833 (2010).
[46] H. I. Amols, C. S. Wuu, and M. Zaider, Radiat. Prot. Dosim. **31**, 125 (1990).